Chemical Engineering Journal 315 (2017) 608–620

Contents lists available at ScienceDirect

Chemical Engineering Journal

journal homepage: www.elsevier.com/locate/cej

A systematic procedure for the virtual reconstruction of open-cell foams

Mauro Bracconi, Matteo Ambrosetti, Matteo Maestri, Gianpiero Groppi, Enrico Tronconi *

Laboratory of Catalysis and Catalytic Processes, Dipartimento di Energia, Politecnico di Milano, via La Masa 34, 20156 Milano, Italy

HIGHLIGHTS

- Structure accounting for variable strut diameter and solid clustering at nodes.
- Geometry based on Voronoi tessellation computed from a random set of points.
- Good agreement between geometrical properties of reconstructed and real foams.
- Complex flow field in real foams effectively reproduced in reconstructed foams.

ARTICLE INFO

Article history:
Received 2 November 2016
Received in revised form 16 January 2017
Accepted 17 January 2017
Available online 19 January 2017

Keywords:
Open-cell foams
Virtual reconstruction
CFD
Voronoi tessellation
Pressure drop

ABSTRACT

Open-cell foams are considered a potential candidate as an innovative catalyst support in many processes of the chemical industry. In this respect, a deeper understanding of the transport phenomena in such structures can promote their extensive application. In this contribution, we propose a general procedure to recover a representative open-cell structure starting from some easily obtained information. In particular, we adopt a realistic description of the foam geometry by considering clusters of solid material at nodes and different strut-cross sectional shapes depending on the void fraction. The methodology avoids time-consuming and expensive measuring techniques, such as micro-computed tomography (μCT) or magnetic resonance imaging (MRI). Computational Fluid Dynamics (CFD) could be a powerful instrument to enable accurate analyses of the complex flow field and of the gas-to-solid heat and mass transport. The reconstructed geometry can be easily exploited to generate a suitable computational domain allowing for the detailed investigation of the transport properties on a realistic foam structure by means of CFD simulations. Moreover, the proposed methodology easily allows for parametric sensitivity analysis of the foam performances, thus being an instrument for the advanced design of these structures. The geometrical properties of the reconstructed foams are in good agreement with experimental measurements. The flow field established in complex tridimensional geometries reproduces the real foam behavior as proved by the comparison between numerical simulations and experiments.

1. Introduction

Open-cell foams are cellular materials made of interconnected solid struts that enclose void regions, named cells, which communicate by means of pores, thus enabling fluids to flow across the structure. The open-cell geometry determines high void fractions resulting in low pressure drops even with high flow velocities. The complex flow field established inside the random and tridimensional geometry increases both the local mixing and the gas-to-solid transport properties, since foam ligaments may result in boundary layer disruption and enhanced mixing [1–3]. Moreover, the typically large specific surface areas allow for high mass transfer rates in the case of catalytically active structures. By considering highly conductive foams, the continuous solid matrix guarantees high axial and radial thermal conductivity, making thermal conduction the dominant heat transport mechanism inside these structures, in particular for systems operating with low conductive fluids and/or low flow rates [4–6]. These features make foams attractive as novel catalyst supports: a great potential is expected, in particular, where heat and mass transport are key factors in the design and operation of the catalytic reactors [7]. Several applications have been investigated in the open literature mainly regarding NOx removal from exhaust gas and catalytic partial oxidation (CPO) of methane to syngas [8–10]. Moreover, foams might be a suitable solution also in highly endothermic, e.g. steam reforming [11], and exothermic systems, e.g. selective oxidation [12,13], methanation and Fischer-Tropsch reactions [14], methanol synthesis [15,16], hydrocarbon hydrogenation reactions [17].

* Corresponding author.
E-mail address: enrico.tronconi@polimi.it (E. Tronconi).

http://dx.doi.org/10.1016/j.cej.2017.01.069
1385-8947/

Notation

Latin letters

d_c	cell diameter [mm]
d_p	pore diameter [mm]
t_s	strut diameter [mm]
t_n	node diameter [mm]
S_v	specific surface area [m^{-1}]
L	sample length [mm]
W	sample width [mm]

Greek symbols

ε	void fraction [–]
ρ	fluid density [kg/m^3]
μ	dynamic viscosity [Pa·s]

Dimensionless numbers

$Re_{d_p} = \frac{\rho d_p u}{\mu}$ Reynolds number based on the pore diameter [–]

Subscripts

rec	evaluated on reconstructed foam
μCT	evaluated with μCT/MRI techniques

Many correlations have been proposed in the open literature to describe the complex geometrical features of open-cell foams and the pressure drop due to flow across such structures. Edouard et al. [18] extensively reviewed the available correlations for prediction of the pressure drop and investigated the performances of the correlations against an extensive set of experimental data covering a wide range of different foams. They stated that the standard deviation between predicted and experimental values might be up to 100%. The description of the transport properties of foams is even more complex resulting in a poor understanding of those phenomena. Despite the considerable potential, this scenario is hampering a wide application of open-cell foams as catalyst supports. Hence, a fundamental analysis of open-cell foams is needed to investigate their properties and behavior. Computational Fluid Dynamics (CFD) is a valuable tool to improve the understanding of open-cell foams, being able to take into account their random tridimensional geometry and to grant deep insights in the complex flow field, enabling detailed analysis of the gas-to-solid transport phenomena. CFD, however, requires the accurate description of the foam microstructural geometry in order to generate the computational domain for CFD simulations. The generation of suitable structures for CFD simulations, with the capability of reproducing both the geometrical properties and the experimental behavior of open-cell foam, is a challenging and crucial task.

Currently, this task has been addressed through two different approaches in the open literature. The first exploits microcomputer tomography (μCT) or magnetic resonance imaging (MRI) techniques to obtain CAD data closely resembling the microstructure of real foams, which can be used to produce the computational domain needed for the CFD simulations [19–22]. The geometries recovered with this method are unique for each sample and might be not representative, in particular, when investigating small foam pieces. Moreover, this approach requires many steps for both the preparation of the sample and the post-processing of the data, resulting in an expensive and time-consuming methodology. The second approach relies on the generation of a virtual microstructure that resembles the real foam structure in terms of geometrical properties. Commonly, this is obtained by the description of a repetitive unit cell consisting of polyhedrons of a well-defined geometry. Lord Kelvin proposed the first deterministic model consisting of tetrakaidecahedrons, i.e. polyhedrons with six square faces and eight hexagonal faces, solving the problem of recovering the space-filling arrangement of cells of equal volume, which minimizes the surface area [23,24]. Several authors have investigated this structure [25–29]. Weaire and Phelan [30] have proposed an improved model consisting of eight cells, six tetrakaidecahedrons and two pentagonal dodecahedrons, which shows a reduction of the surface area of 0.3%. The simulations of pressure drop across these repetitive and ordered structures usually underestimate the experimental values by 30% [31]. Other unit cell models can be found in the open literature, such as the ordered cubic structure [1] or the dodecahedral unit cell model [32]. These structures have been exploited to derive correlations for the geometrical features and transport properties, whereas no application in the field of CFD simulation of real open-cell foams is reported in the available literature. Deterministic ensembles of unit cells do not account for the stochastic nature of the real foam structure, resulting in deviations between numerical and experimental behaviors mainly due to the preferential flow pattern established in the regular geometry. Therefore, it is necessary to take into account the characteristic randomness of real foams. Habisreuther et al. [33] and Lucci et al. [34] proposed to randomize the perfectly ordered Kelvin structure by means of a stochastic displacement of nodes. These methods allow for a good description of the specific surface area, but show significant deviations in the prediction of the transport properties. On the other hand, Gibson and Ashby [35] proposed the Voronoi tessellation as a candidate method to generate the foam structure, since it satisfies the topological requirement on edge and face connectivity [36]. Moreover, Roberts and Garboczi [37] analyzed different stochastic approaches, such as sphere overlapping, Voronoi tessellation, Gaussian random fields, ellipsoid overlapping. They stated that the Voronoi tessellation shows a microstructure similar to the open-cell foam geometry. Along these lines, Randrianalisoa et al. [38] exploited the Laguerre-Voronoi tessellation to generate open-cell structures and analyzed the pure heat conduction phenomena assuming a circular cross-sectional shape with promising results. Wehinger et al. [39] proposed a methodology to reconstruct foams using the Voronoi tessellation, assuming the pore diameter as the characteristic length. A good agreement with experimental geometrical data for foams with a porosity up to 0.85 was claimed, but a very poor description of the fine ligaments structure was adopted. The strut cross-sectional shape, circular and trapezoidal, respectively, was kept constant without taking into account any variation with the void fraction. Moreover, the material clustering at the nodes was neglected by assuming a constant strut diameter.

In structures as open-cell foams, the transport properties strongly depend on the peculiar morphology and on the local modifications of the microstructure. Hutter et al. [39] showed that strut thickness and shape influence the mixing properties of the foam structure. Kanaun and Tkachenko [40] elucidated the effect of the variations of the strut size on the effective solid thermal conductivity. Hence, the accurate description of these properties, i.e. strut cross-sectional shape, constrictions, solid clustering at nodes, is an essential aspect for an accurate reproduction of real foams behavior.

In this work, we establish a systematic methodology for the digital reconstruction of a realistic foam structure. The reconstructed foams show the same topology, e.g. number of faces per cell, and geometrical properties, e.g. different strut cross-sectional shapes,

of a real foam. Moreover, the procedure is able to reproduce the realistic solid distribution inside open-cell foams by considering material clustering at nodes and variable strut diameter, a key feature for the correct description of the transport properties. The methodology requires only a few pieces of information as input, i.e. either the cell or the pore diameter, the void fraction and the strut cross-sectional shape. These data can be easily measured by optical microscopy and by pycnometric methods, avoiding other time-consuming and expensive experimental techniques. Our methodology exploits the Voronoi tessellation for the generation of the foam skeleton in order to reproduce the bare structure of the foam sample. Since the strut geometry assumes a great relevance for the geometrical and fluid-dynamic properties, a faithful description of struts and nodes is required. We take into account both the strut cross-section and the solid clustering in order to generate an accurate virtual reconstruction of the real foams. The goal is also to develop a useful tool for the advanced design of these structures enabling a CFD analysis of many foam samples and an optimization of the geometry based on numerical simulations to suit the necessities of the investigated process. In future works, we will investigate the heat and mass transport properties exploiting this geometrical reconstruction, in order to assess the adequacy of the virtual reconstruction methodology also in the description of the transport processes.

The paper is organized as follows. In the first part, the reconstruction procedure is presented. In the second part, the capability of the procedure to generate real foam structures is investigated by comparing the reconstructed sample with experimental information available in literature for what concerns geometrical features and pressure drops.

2. Reconstruction procedure

Real foams are an irregular packing of space-filling polyhedrons and contain cells of different size and shape with different numbers of faces and edges [41]. The complex solid geometry can be characterized by means of its morphological parameters, i.e. cell diameter, pore diameter and strut thickness, as depicted in Fig. 1. In the present work, the cell diameter is identified with the size of a sphere totally inscribed inside the open-cell, while the pore diameter is the size of the windows connecting adjacent open-cells. The accurate description of the foam structure has to consider the ligaments cross-sectional shape, which can move from circular to triangular and, by considering highly porous metal foams, even triangular concave, as the void fraction is increased [28]. Herein, the strut thickness is considered as the diameter of the circular ligaments or the side of the triangular ones, respectively, in the middle point of the strut. On the other hand, the node diameter is identified with the diameter of the circular ligaments or the side of the triangular one at the node-strut junction. Moreover, it is necessary to take into account the material clustering at nodes resulting in a non-uniform strut profile along its axial direction, as shown in Fig. 1. Additional information usually available includes the porosity, i.e. the ratio between the void and the total volume, and the specific surface area, i.e. the ratio between the accessible surface and the total volume.

In this work, the cell diameter is assumed as the characteristic length of the reconstruction since it describes well the dimension of the unit cells building the structure and the experimental measurements show a narrow distribution around the average value. When this experimental information is not available, the pore

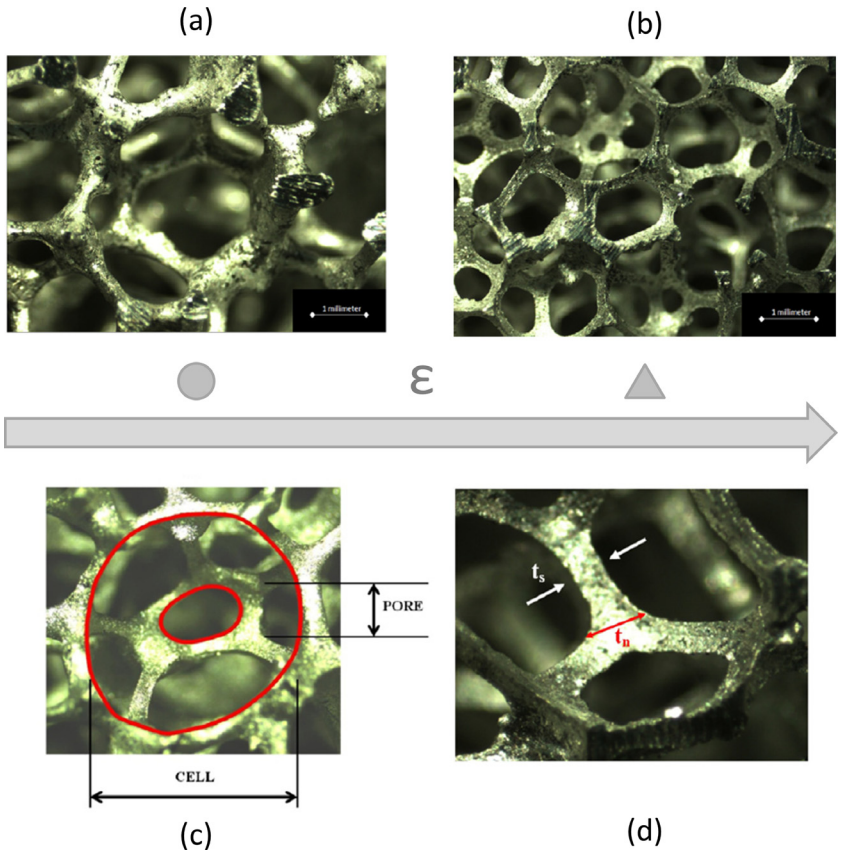

Fig. 1. Cell structure of common foams with circular (a) and triangular (b) cross-sectional shape of the strut according to foam porosity; identification of cell and pore diameters (c); definition of strut and node dimensions (d) (pictures from [41]).

diameter is usually known or can be estimated by considering the PPI information supplied by the manufacturer. In this case, a tentative cell diameter is guessed from the measured pore diameter and the foam is reconstructed. Then, the pore size in the reconstructed foam is evaluated and the procedure is iterated until convergence on the pore diameter is reached.

The reconstruction procedure consists of the three following steps:

a) Determination of cell centers by packing a random bed of spheres of constant diameter equal to the characteristic length.
b) Generation of foam skeleton by exploiting the Voronoi tessellation to recreate a realistic bare structure.
c) Reconstruction of the foam structure by inserting in the bare structure the struts and the nodes properly modeled to accurately reproduce the real geometry and by adjusting the foam porosity to match the experimental value.

2.1. Determination of cell centers

The first part of the algorithm is the determination of an initial set of points, which represent the seeds of the Voronoi tessellation. This is obtained by randomly packing a bed of spheres. According to the literature, discrete element method (DEM) [42] and Monte Carlo simulations [43,44] can be exploited to generate a packed bed of spheres. In this work, the generation of the random packing is carried out by means the DEM methodologies with the open source code LIGGGHTS [45]. In the DEM method, spherical monodisperse particles are randomly initialized within a square-based tubular domain and fall because of gravity to the bottom of the tube. For each of these particles a force balance is formulated and solved taking into account the gravity force and the interactions between particles and between the particles and the tube wall. The DEM simulation stops when steady state conditions (i.e. zero velocity for the entire set of spheres) are reached. The properties of spherical particle are taken from Ookawara et al. [46]. The diameter of the sphere is equal to the characteristic length, which is represented by the cell diameter of the foam structure.

The dimensions of the cylindrical domain are determined to avoid wall-effects on the void fraction of the packing. For mono-distributed spheres, the influences of the confining wall occurs for five to seven sphere diameters [47]. Hence, a tube-to-particle diameter ratio of 15 is defined and only the central region is considered for further steps. Zou and Yu [48] investigated the variation of the void fraction in the axial direction showing that the effect of the bed height has to be considered when the thickness is relatively limited. The initial and final portions of the bed, i.e. a thickness equal to five cell diameters, are neglected to avoid axial variation of the void fraction. The initial bed of spheres is shown in Fig. 2(a) along with the selected portion for the foam generation, see Fig. 2(b) and (c). Once the packing is settled, the positions of the centroids are extracted, as shown in Fig. 2(d).

2.2. Generation of the foam skeleton

The second step of the procedure is the generation of the cell skeletons. We exploit the Voronoi tessellation to generate the foam bare structure, since it divides the spaces in a set of space-filling polyhedrons with no-holes and no-overlaps. Starting from an initial set of seed points, obtained by packing a bed of spheres, the Voronoi algorithm subdivides the space in such a way that each Voronoi polytope encloses all the points of the space that are the closest to the seed. Being given a spatial domain $D \in R^3$, a set of seeds $S_i(\boldsymbol{x}_i)$, where $\boldsymbol{x}_i$ is the position vector of the seed i, and defined a distance function d, every point S_i has associated a Voronoi polyhedron V_i as follows:

$$V_i = \{P(\boldsymbol{x}) \in D | d(P, S_i) < d(P, S_j) \forall i \neq j\} \quad (1)$$

where $P(\boldsymbol{x})$ is the position vector of a general point in D.

In this work, the distance function d is assumed as the Euclidean distance and the set of seed points is obtained from the random packing of spheres of fixed diameter. The tessellation is generated exploiting the open-source library *voro++* [49] and imposing cyclic boundary conditions at the border of the domain. The Voronoi algorithm generates around each seed a convex polyhedral unit-cell made of vertices, joined by edges delimiting planar faces, which connect neighboring cells. The vertices of the entire set of unit-cells are memorized in a list to generate the nodes of the foams. Each vertex is linked to a well-defined number of neighbors by means of edges, which are stored to subsequently generate the struts.

Once this procedure is completed, the foam skeleton is completely established as shown in Fig. 3.

2.2.1. Generation of the foam structure

Foam microstructure is complex and shows many local irregularities which cannot be deterministically reproduced, since they are peculiar features of the portion of the investigated sample. At the same time, the overall effect of these irregularities on the geometrical and transport properties can be averaged by considering a sample of sufficient size, i.e. larger than the representative elementary volume (REV) [50]. In this case, their effect on the overall

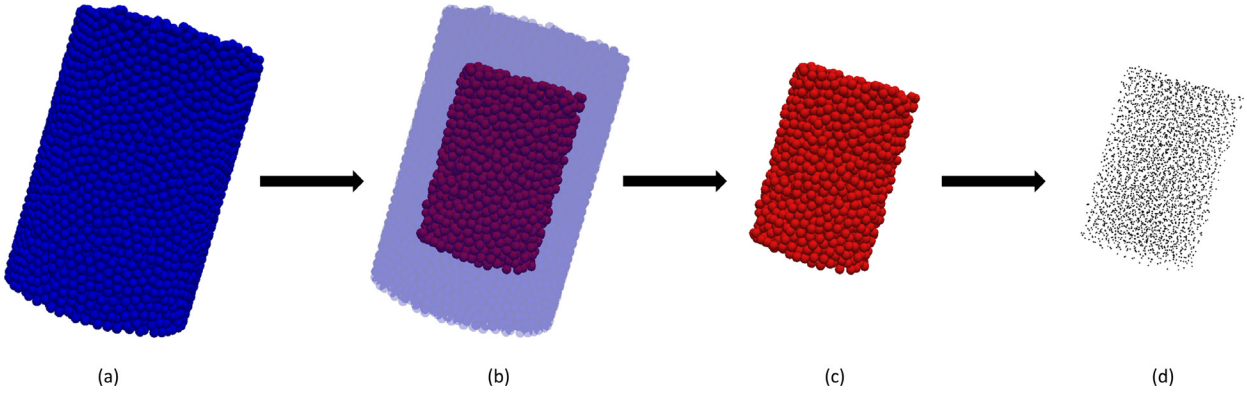

Fig. 2. Determination of cell centers: initial packing of spheres (a), portion of the packing (in red) selected to avoid wall effects on the void fraction (b), set of spheres considered for the evaluation of the cell centers (c) and extracted centers of the spheres acting as the cell centers and as the seed points of the Voronoi tesselation (d).

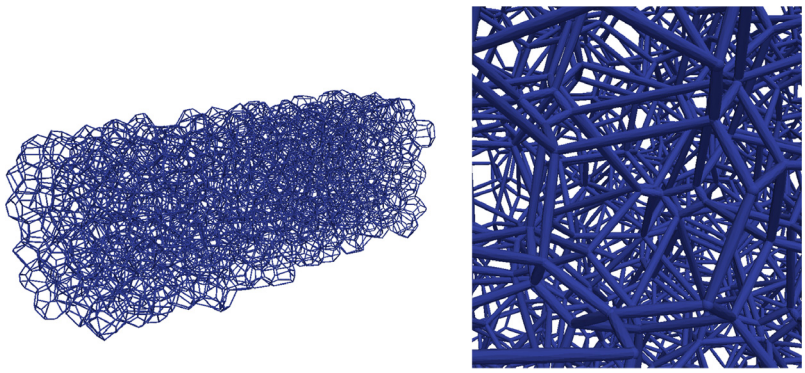

Fig. 3. Foam skeleton representing the interconnected polyhedrons from the Voronoi tessellation (a) and detail of the foam skeleton focusing on the interconnections between vertices of the Voronoi polyhedrons (b).

geometrical properties becomes negligible in respect to the effect of such macroscopic properties as the void fraction and the specific surface area. Obviously, the influence of the microstructure plays a crucial role in the correct description of the fluid flow and, thus, of the transport properties, but the effect of the local irregularities is, once again, negligible in respect to overall effects induced by the geometry. Thus, the accurate description of nodes and struts is crucial to generate a final foam structure, which properly reproduces the influence of the geometry on the transport phenomena. Despite this, the reproduction of the local irregularities is not required since their effect on the overall properties become negligible by considering a sample of sufficient size. Experimental evidence shows that the ligaments shape depends on the void fraction. The strut cross-section moves from circular to triangular by increasing the porosity. Thus, two different shapes for the ligament cross-section are proposed according to the void fractions of the real foam. Moreover, solid material clusters at nodes, thus a variable strut thickness along the axis is required. We propose a second order polynomial profile to describe the variations of the strut thickness both with the circular and triangular cross-sections. The strut and node diameters are guessed by exploiting a simple geometrical model whose outputs are used as an initial estimate in the foam generation procedure. In this geometrical model, four ligaments join at each node forming an angle of 109.5 degrees according to Plateau's laws [51], which is the theoretical angle reached at the thermodynamic equilibrium in liquid foams. Thus, the foam structure is considered as a collection of those ideal nodes connected to each other by means of parabolic struts. The nodes are modeled as spheres or as tetrahedrons depending on the strut cross-sectional shape, whereas the struts are represented by paraboloids with either circular or triangular cross-section. In both cases, the strut and node diameters are recovered by considering two physical constraints. The first constraint imposes continuity and smoothness at the strut-node junction. This condition firstly determines that the strut and the node share the same local diameter at the junction. Moreover, the derivative of the strut-node profile has to be continuous in each point along the axis and, in particular, at the junction. Thus, the constraint imposes an analytical relationship between the strut and node diameter. As the second constraint, we assume that the total solid volume loaded in the foam structure entirely belongs to struts and nodes. In particular, the total solid volume equals the overall sum of the volume of nodes and struts determined by the vertices of the Voronoi tessellation. The strut volume is evaluated by considering both the cross-sectional shape and the parabolic profile. The foam skeleton generation provides the position and the connectivity of each vertex by defining the edges of the polyhedrons. A portion of the nodes and the effective development of the strut constitute the polyhedron edge. Thus, the ligament length is equal to the distance between the polyhedron vertices after removing the contribution of the nodes. Hence, the strut volume is equal to the volume of the paraboloid of well-defined length, e.g. the effective length of the ligament, and sizes, e.g. the node and strut diameter. The node volume is computed by considering the node geometry and, in the case of circular strut, by removing the spherical cap which overlaps the strut in order to avoid double evaluation of those volumes. The geometrical model allows for the initial estimation of the node and strut diameters, which are used to generate an initial structure by inserting the representative geometries for them in the Voronoi foam skeleton. The foam structure is numerically described by a set of triangles, which cover the entire surface and are completely defined by the vertices and the normal unit vector in respect to the face center, using the Standard Tessellation Language (STL). The number of triangles tessellating the geometrical surface has been defined to recover a structure whose geometrical features are independent of the adopted discretization.

Since the node and strut diameter are evaluated by assuming a simple and ideal geometrical model, small deviations between the void fraction of the reconstructed foam and the experimental value might be experienced. Thus, the porosity of the final foam structure is adjusted by shrinking or enlarging the structure to close the gap between experimental and predicted values. In particular, each vertex of the triangles shifts along its unit normal vector with respect to the foam surface to preserve the strut cross-sectional shape of the strut, increasing or reducing the solid material to match the experimental porosity.

The foam structure, see Fig. 4, is finally exported in STL format, which can be easily imported in a CFD meshing software to generate the computational domain.

3. Results and discussion

3.1. Geometrical parameters

The capability of the reconstructed foams to reproduce the morphological parameters of the real structure is crucial for the description of transport phenomena. The validation of the procedure, given in Section 2 above, is carried out by means of the comparison between the geometrical properties of virtually generated

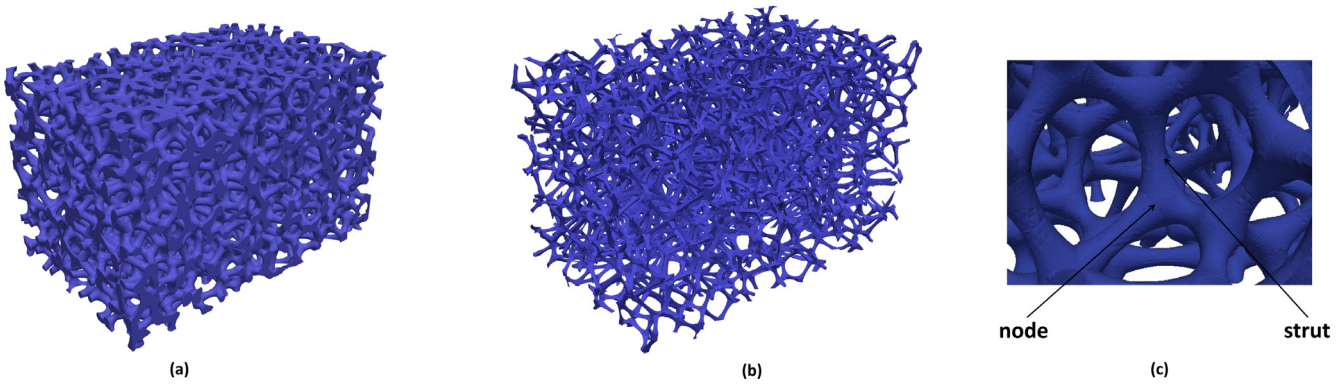

Fig. 4. Final reconstructed foam samples with circular (a) and triangular (b) struts along with a detail of the strut-node junction in the case of circular strut cross-section shape (c).

foams and experimental data [28,41,52–56]. Several samples have been considered to investigate the adequacy of the methodology on foams covering a large range of void fractions, from 0.72 to 0.95, a large range of pore sizes, from 10 to 45 PPI, and different strut shapes, as listed in Table 1. The reconstructed sample size is greater than the representative elementary volume (REV) proposed in literature [41,50], i.e. three cell diameters in each direction, in order to be representative and to obtain results comparable with μCT/MRI data.

3.1.1. Analysis of the foam geometry

The Voronoi tessellation produces a set of polyhedrons, which completely fill the space and generate the open-cells. The number of faces is an important feature since it represents the number of openings in each cells corresponding to the pores of the structure. The correct description of the cell interconnectivity is an important parameter for the description of the flow field since the number of pores contributes to the establishment of the flow field. Real foams show a distribution for the number of faces of the open-cells. In their review on cellular solids, Gibson and Ashby state that the average values for a foam-like structure is around 14 [35]. However, this value is not a requirement and, usually, the number of faces depends on the manufacturing process [35]. The reconstructed foams have been analyzed in order to investigate the results of the procedure in comparison to experimental data. First, the number of faces in each cell has been evaluated in the bare structure directly generated by the Voronoi tessellation. The results are reported in Table 2. The average value is slightly larger than 14 and in agreement with literature data for Voronoi tessellations [36,57]. Then, the same analysis has been carried out on the final reconstructed foams, which show an average value of 12.3 in agreement with experimental measurements of polymeric and metallic open-cell foams which report values between 12.5 and 13.7 [58–61]. The average number of faces of reconstructed foams is different from those recovered for minimum surface energy polyhedrons, e.g. Kelvin or Weaire-Phelan structures, and this is also consistent with literature data [58]. On one side, the number of open faces is independent of the PPIs as occurs in real metal foams [59]. On the other side, Fig. 5 shows a linear trend in the number of openings, which increases by moving from low to high porous foams. The presence of struts determines that some of the faces of the initial Voronoi structure could become closed due to the overlap between the ligaments surrounding the pore. This can occur especially considering very small openings between cells, which are present in the Voronoi structure [36]. This behavior is emphasized in low-porosity foams where the significant dimension of struts could close a larger fraction of those faces. This trend is not widely reported in literature, where the experimental results typically cover a small range of void fractions and are focused on foams with high void fractions. Nevertheless, these experimental results reasonably match the results of the digital reconstruction herein reported as shown in Fig. 5.

The strut-to-strut angle can give further insight in the foam geometry. The average value for the reconstructed foam samples

Table 1
Properties of studied foam samples determined by μCT measurements (data from [28,41,52,54–56]).

Foam sample	PPI	ε [-]	d_c [mm]	d_p [mm]	$S_{v,\mu CT}$ [m^{-1}]
A[a] [41]	40	0.890	2.45	1.29	936
B[a] [41]	10	0.897	3.58	1.83	649
C[a] [53]	45	0.783	–	0.65	1816
D[a] [53]	20	0.719	–	1.02	1260
E[a] [28]	30	0.862	–	1.07	1136
F[a] [52]	30	0.807	–	0.86	1422
G[a] [52]	30	0.766	–	0.89	1438
H[a] [54]	30	0.806	–	0.88	1402
I[a] [54]	45	0.757	–	0.63	1884
L[b] [55]	10	0.951	5.23[c]	2.61[d]	380
M[b] [55]	10	0.937	3.46[c]	1.69[d]	675
N[b] [55]	20	0.913	3.15[c]	1.53[d]	720
O[b] [56]	20	0.920	4.60	–	510
P[b] [56]	5	0.913	4.24	–	590
Q[b] [56]	10	0.962	4.20	–	440

[a] Strut with circular cross-sectional shape
[b] Strut with triangular cross-sectional shape
[c] Average cell diameter
[d] Data from [62]

Table 2
Geometrical properties of the reconstructed foam samples and comparison of the specific surface areas with measured values from literature [28,41,52–54,56,62].

Foam sample	ε [–]	Average number faces Voronoi	Average number faces reconstructed	Strut-to-strut angle [°]	$S_{v,rec}$ [m^{-1}]	$S_{v,\mu CT}$ [m^{-1}]	S_v Deviation [%]
A[a]	0.890	14.30 ± 1.19	12.31 ± 1.12	111.7	932.0	936.0	0.4
B[a]	0.897	14.26 ± 1.17	12.32 ± 1.04	111.5	645.0	649.0	0.6
C[a]	0.783	14.30 ± 1.27	11.48 ± 0.98	111.7	1806.7	1816.0	0.5
D[a]	0.719	14.27 ± 1.20	10.84 ± 0.92	111.6	1174.5	1260.0	6.8
E[a,c]	0.862	14.33 ± 1.26	12.18 ± 0.97	111.7	1103.5	1136.0	2.9
F[a]	0.807	14.35 ± 1.23	11.56 ± 0.94	111.9	1373.1	1422.4	3.5
G[a]	0.766	14.26 ± 1.26	11.34 ± 1.01	111.7	1391.9	1437.8	3.2
H[a,c]	0.806	14.24 ± 1.29	11.22 ± 0.95	111.8	1364.4	1402.0	2.8
I[a,c]	0.757	14.35 ± 1.22	11.11 ± 0.89	110.9	1939.7	1884.0	3.0
L[b]	0.951	14.26 ± 1.22	13.02 ± 1.02	110.6	376.2	380.0	1.0
M[b]	0.937	14.33 ± 1.22	12.58 ± 1.19	111.8	631.0	675.0	6.5
N[b]	0.913	14.32 ± 1.22	12.52 ± 1.22	110.8	724.0	720.0	0.6
O[b]	0.920	14.33 ± 1.22	12.49 ± 1.07	111.8	547.2	510.0	7.3
P[b]	0.913	14.29 ± 1.21	12.48 ± 1.05	111.7	611.6	590.0	3.7
Q[b]	0.962	14.31 ± 1.25	13.31 ± 1.15	111.8	406.0	440.0	7.7
Average		14.29 ± 1.23	12.28 ± 1.04	111.4			

[a] Strut with circular cross-sectional shape
[b] Strut with triangular cross-sectional shape
[c] Foam structure for CFD simulations

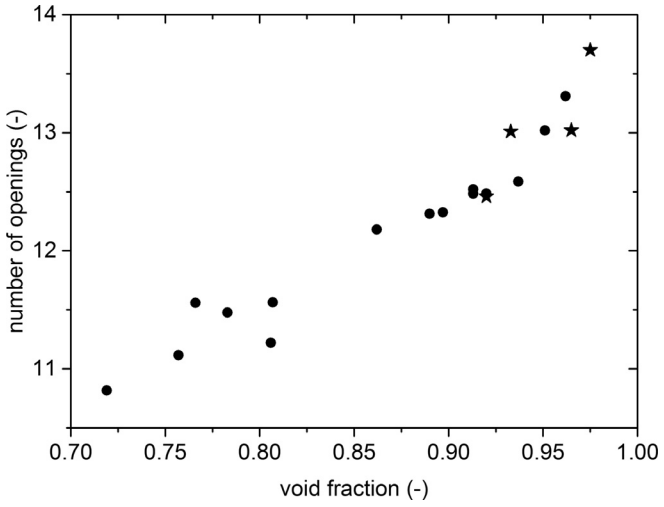

Fig. 5. Number of openings per foam cell as a function of the void fraction for reconstructed foam (circle) and experimental measurements (star) [55–58].

is 111.4°, as reported in Table 2, close but larger than the tetrahedral angle of 109.5° at which four ligaments meet in an equilibrium structure, as depicted by Plateau [36]. Deviations of the same order of magnitude are reported in literature for polyurethane foams [58] and they can explain the different number of faces in ideal geometries and reconstructed samples. It is worth emphasizing that the initial Voronoi geometry well describes the soap froth structure, described by the bare foam geometry. On the contrary, it shows some different geometrical properties in respect to real solid foams. However, the insertion of the solid ligaments and the accurate description of the clustering at the nodes affect topology and structure of the Voronoi polyhedrons. In fact, they introduce a certain degree of local irregularities, such as closed pores or merged struts, which are usually present in real samples, in particular at low porosities, allowing for the accurate reproduction of solid foam properties.

3.1.2. Analysis of the mean pore diameter

The pore diameter has been investigated by measuring the opening, which allows the fluid to flow from one cell to another. This analysis has been carried out for the foams whose geometrical properties are completely known [41,62], covering a range of void fraction between 0.89 and 0.95. The reconstruction procedure for those foams is based on the measured cell diameters enabling the comparison of the pore size estimated on the virtual foams with experimental values. A large foam volume consisting of at least 50 cells resulting in more than 500 pores has been considered as a representative sample. To carry out the analysis, the computational domain is generated starting from the reconstructed foam and the mesh is segmented in order to mark each computational cell with a unique label representative of the foam cell owner.

The cell centers already exploited for the generation of the reconstructed foam are used as initial seeds for the Voronoi tessellation algorithm. Each mesh cell is, then, paired with the corresponding Voronoi polyhedron, as shown in Fig. 6(a). Thus, each computational cell is labelled with a distinct number depending on the Voronoi cell in which it is contained. Once the entire set of cells is labeled, the region of the computational domain where the label changes are identified as pores, as shown in Fig. 6(b). The open-cells considered to carry out the evaluation of the pore diameter are the ones entirely contained inside the foam volume. Once the pore network is completely identified, the overture diameter is evaluated as proposed by Al-Raoush [63]. The center of the pore is computed and the radius is evaluated as the geometric average of the distances between the pore surface and the pore center. The average pore size shows a fair agreement with measured data [41,62], as reported in Table 3, with deviation less than 10%. The independence of the results from the background bash has been verified by decreasing the grid size until convergence.

3.1.3. Analysis of the specific surface

The specific surface area is a key parameter in the description of the transport properties since it governs the fluid-solid interactions. An accurate description of this property is a crucial requirement for such a reconstruction. In order to validate the procedure, the specific surface area of the reconstructed samples is compared to measured data available in literature in a large range of porosities, from 0.7 to 0.96, and PPI, from 5 to 40. The strut cross-sectional shape, required as an input of the reconstruction procedure, has been defined according to experimental evidence or by assuming the shape according to the void fraction, following to the indications reported by Inayat et al. [28].

In Fig. 7, a parity plot illustrates the reconstruction results versus the measured values obtained by μCT or MRI techniques [41,52–56,64]. The deviations between the measured specific surface area and that evaluated on reconstructed foams are typically

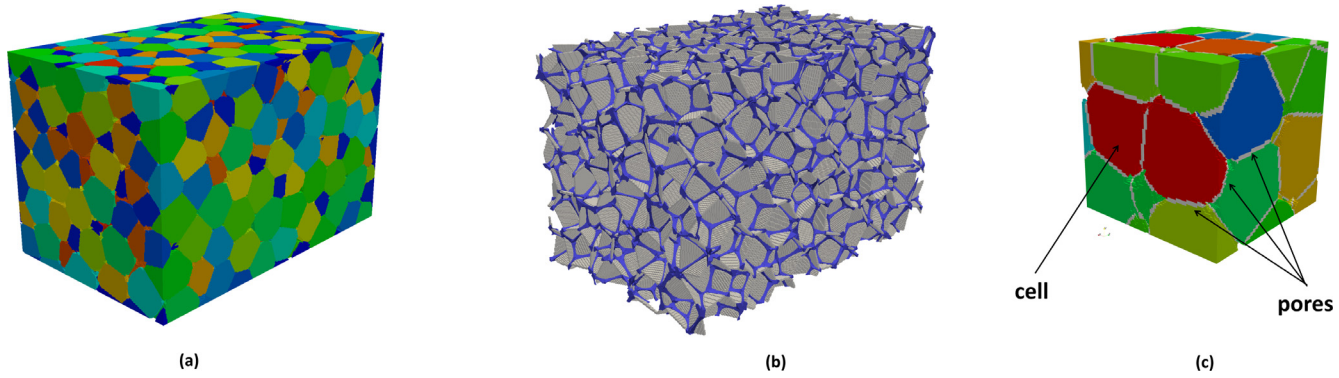

Fig. 6. Pore size analysis on a reconstructed foam: segmentation of the geometry in order to identify open-cells (a), depiction of the pores entirely owned in the sample (b) and detail of segmentation with highlighted the cells (coloured according to the cell volume) and the pores (grey surfaces) (c). (For interpretation of the references to colour in this figure legend, the reader is referred to the web version of this article.)

Table 3
Pore diameter of reconstructed sample versus experimental value from μCT [41,62].

Foam sample	$d_{p,\ \mu CT}$ [mm]	$d_{p,rec}$ [mm]
A	1.29	1.15
B	1.83	1.66
L	2.61	2.64
M	1.69	1.69
N	1.55	1.55

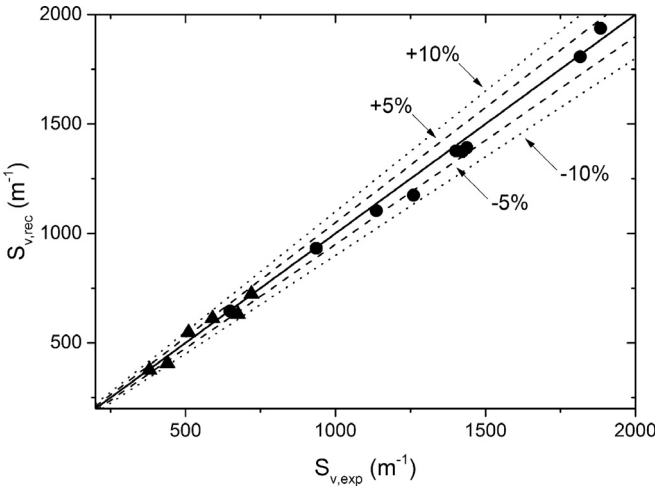

Fig. 7. Parity plot comparing the specific surface area of the reconstructed foam and the experimental values for circular (circle) and triangular (triangle) foams (experimental data from [41,48–50,59,61]).

less than 5%, as reported in Table 2. The largest error for the circular and triangular shapes are 6.8 and 7.3%, respectively. Samples L, M, N have been experimentally investigated by adopting different voxel resolutions equal to 40 [55] and 8.5 [62] μm, respectively. The specific surface areas change by increasing the resolution of the images due to the higher capability in describing the surface roughness of the sample, whereas the low-resolution images smooth the surface of the reconstructed sample [65]. Our procedure is able to generate smooth surfaces only since no roughness is introduced in the tridimensional model, thus the comparison between the reconstruction and tomographic measurement are carried out on the low-resolution data.

The good agreement for the specific surface area, as well as for the other geometrical properties, confirms the capability of the proposed methodology to correctly reproduce the complex tridimensional geometry of real open-cell foams.

3.2. Pressure drop

The simulation of the complex flow field in open-cell foams is critical for the correct description of transport phenomena. Hence, pressure drop calculations have been carried out on the reconstructed sample in order to assess the capability of the procedure to generate structures that are totally representative of the foams properties. Measured data from open literature [54,64] of foams of different porosities, pore size and materials are considered.

For general porous media different flow regimes are established inside the structure [66]:

- Darcy or creeping flow regime ($Re_{d_p} < 1$)
- Forchheimer flow regime ($1 < Re_{d_p} < 150$)
- Post-Forchheimer flow regime, i.e. unsteady laminar flow, ($150 < Re_{d_p} < 300$)
- Fully turbulent regime ($Re_{d_p} > 300$)

where Re_{d_p} is the Reynolds number based on the pore diameter of the open pores of the foam structure.

These regimes were initially derived for flow within packed beds consisting of spherical or cylindrical pellets. Therefore, the exact transferability of these ranges to the open-cell foams is questionable. Thus, these thresholds are approximate points of reference, which can be exploited to carry out a first classification of the possible regimes. Accordingly, the threshold Reynolds number, where the transition to turbulence appears, varies with respect to the different geometries adopted for experimental activity from 300 to 400 [39]. The existence of macroscopic turbulence in porous media is controversial in the literature. Jin et al. [67] investigated the existence of macroscopic turbulence inside porous structures by carrying out direct numerical simulations (DNS) on regular porous matrices. They suggest that the size of turbulent structures do not extend far beyond the pore scale since the solid matrix dampen any macroscopic turbulence. Recently, Meinicke et al. [68] showed the development of flow instabilities when the Reynolds number was larger than 500 due to the presence of the incoherent and strongly fluctuating flow structures. Della Torre et al. [69] showed that the pressure drop could be reasonably predicted by adopting a laminar and steady-state numerical setup even in seemingly turbulent conditions. Along these lines, the simulations are performed across the entire range of Reynolds numbers in order to compare the predictions based on the reconstructed foams with experimental values in every flow regime. The reconstructed foams selected are Sample E, H, I, which cover a range of porosities from 0.76 to 0.86 and of pore densities from 30 to 45 PPI.

3.2.1. Numerical modeling and computational domain

The operating conditions adopted in the simulations are the same of the experiments [54,64], as listed in Table 4. In these conditions, the simulations cover a range of empty tube velocities from 0.5 to 8 m/s, which correspond to Reynolds numbers evaluated on the pore diameter from 20 to 450. The working fluid is air and is modeled as an incompressible perfect gas because of the low Mach numbers (Ma < 0.1) and the isothermal conditions. The simulations are performed with simpleFoam, a numerical steady-state solver part of the OpenFOAM framework [70], developed for steady-state incompressible laminar and turbulent flows adopting the SIMPLE algorithm [71]. The simulation of the fully turbulent regime has been carried out exploiting both laminar and Reynolds Averaged Navier-Stokes (RANS) approaches. Among the several turbulence models, the low-Re k-ωSST model was selected because it is more flexible in wall-bounded flows [72,73]. We obtained similar results for pressure drops adopting both numerical set-ups, as already found by Della Torre et al. [69].

The foam samples adopted for the experimental activity are usually of large dimensions in both the stream-wise and transverse directions. The numerical reproduction of such a large sample is unfeasible due to the large amount of requested computational resources. As we are interested in a fully developed flow regime, we considered periodic boundary conditions and symmetric boundaries along the stream-wise and the transverse direction, respectively. In this way, it is possible to reproduce the behavior of a large sample by analyzing a reduced but representative portion of the foam. Obviously, the velocity locally varies in both the longitudinal and the transverse directions in the real tridimensional foam structure. No local periodicity could be observed in the flow fields inside the structure, since the geometry is stochastic and any periodic geometrical repetitions are experienced. However, assuming that the void fraction and the specific surface area are uniform along the sample, the fully-developed macroscopic behavior of the flow may be well described, in particular addressing our attention to pressure drops, by considering a stream-wise periodic structure with length L represented by a sufficient number of open-cells. By extracting a section in the fully-developed region, the previous portion macroscopically affects the flow field as the region under investigation allowing for this simplified description of the computational domain without any loss in accuracy. This approach has been exploited to carry out fluid-dynamic simulations across geometrical periodic structures with good results [39].

For the generation of the computational domain, snappyHexMesh, an open-source software provided within the OpenFOAM toolbox [70], has been used to create the fluid mesh. Mesh convergence analysis has been carried out in order to ensure independence of the pressure drop results from the computational domain. The mesh is refined near the wall and then snapped on the foam surface, in order to reconstruct the geometry with adequate accuracy. Several computational grids have been generated with an increasing level of detail until the independence of the pressure drop in respect to the computational domain was reached. One example of the mesh convergence study is depicted in Fig. 8(a). The dimensions (e.g. length and width) of the investigated samples are given in Table 4. At the outlet section, a Dirichlet boundary condition has been assigned to the pressure field, whereas a Neumann boundary condition has been used for k and ω in RANS simulations. At the inlet section, Neumann boundary conditions are imposed for the pressure field. The walls of the struts are no-slip walls taking into account the zero velocity of the fluid on the solid surface, whereas a Neumann boundary condition is imposed for pressure. Cyclic boundary conditions along the stream-wise direction are imposed for the velocity. Symmetric boundary conditions are imposed in the transverse directions for all the variables. An example of the computational domain is

Table 4
Operating conditions for CFD simulations of pressure drop along with dimensions of reconstructed samples.

Foam sample	Fluid	T [°C]	Foam width W [mm]	Foam length L[mm]
B	Air	20	9.0	33.4
E	Air	20	13.4	20.7
H	Air	40	13.2	22.6
I	Air	40	9.4	16.0

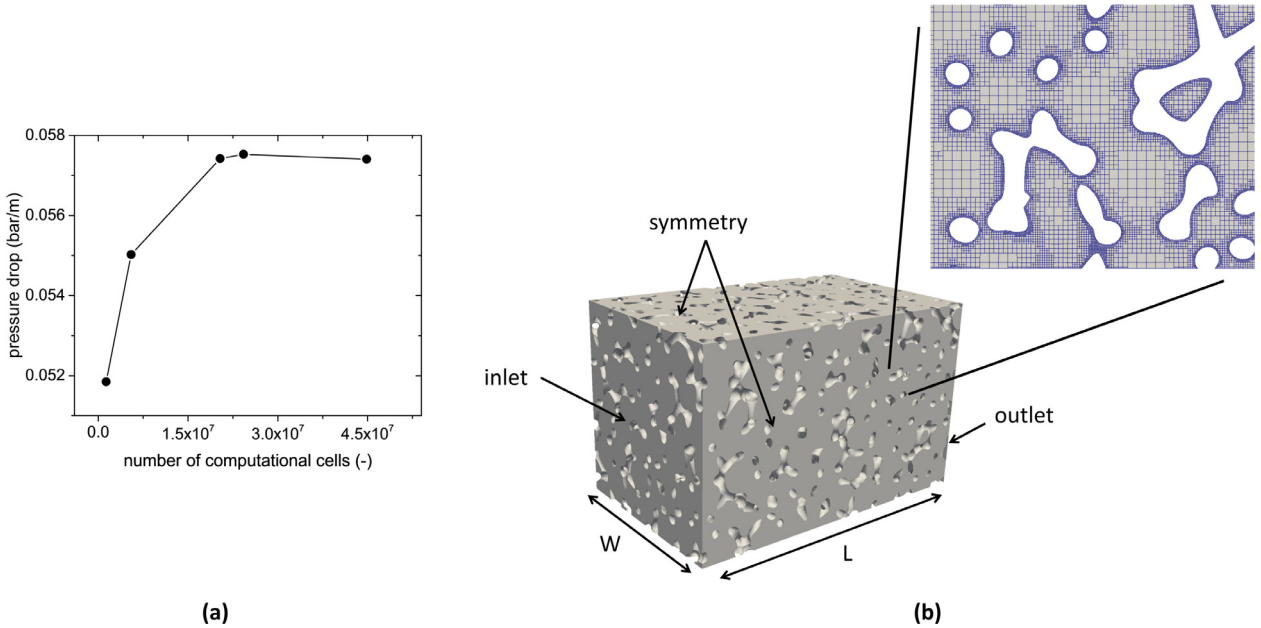

Fig. 8. Mesh convergence study for Sample H at an empty tube velocity of 2 m/s (a) and an example of the computational domain for CFD simulation of pressure drops with an insight of the computational grid (b).

shown in Fig. 8(b) along with a detail of the computational domain around a strut.

A second order upwind scheme (linear upwind) was adopted for the discretization of the convective terms. Using a 64-core CPU with 128 GB RAM, parallelized steady-state calculations took approximately 4 h each. The solution was considered to be well converged when reaching residual values of 10^{-5} for each flow variable.

3.2.2. Simulation results

The effect of the number of foam cells in the stream-wise direction has been first investigated to obtain pressure drop estimates independent of the length of the computational domain.

The analysis elucidates that 10 cells are sufficient to obtain an independent solution, as shown in Fig. 9. By looking at the specific surface area with respect to the number of foam cells in the stream-wise direction, it is evident that once the independence of this property is reached, the pressure drop becomes constant with the number of cells. The unit cells obtained from the Voronoi algorithm statistically have the same geometrical features. Despite this, the local morphology of the cells can differ due to particular geometry of the polyhedrons characterized by a number of faces in a range between 7 and 20 [36]. These local differences can increase or decrease the surface area of the struts, since the number of edges and their length are function of the number of faces, until this effect is averaged by considering a sufficient number of cells.

In a previous work [41], the tomographic scans of Sample B were performed and its tridimensional structure was digitally reconstructed. To assess the capability of the reconstructed foams to reproduce the real flow field, the pressure drops evaluated on the Voronoi-based geometry are compared with the results of the same simulations carried out on the real sample geometry obtained by μCT. The virtual and tomographic reconstructed samples have the same dimensions and experience the same flow conditions. The computational domain adopted for the two different reconstructions is generated with the same features in order to have comparable results. Moreover, the same numerical setup is adopted for the two simulations. The simulations show that the agreement between the pressure drops evaluated on the two structures is fairly good, as depicted in Fig. 10. A slight overestimation at high Reynolds number is experienced due to the different open-cell structures, which affect the form drag term, relevant at high flow velocities. In particular, the real foams present slightly larger pores and some peculiar cluster of solid material, which are not present in the virtual foam geometry. Despite the small differences in the microstructure, the predictions of tomographic and Voronoi-based foams deviate less than 5%, showing the capability of the reconstructed geometry to macroscopically interact with the flow field as the real foams.

The numerical pressure drops are compared to experimental data reported in the open literature [54,64] in Fig. 11.

The pressure drop evaluated in CFD simulations are usually in good agreement with experimental values. Some deviations are experienced at high velocities, in particular for Sample H, where the simulations underestimate the experimental values. The symmetric boundary conditions adopted for the simulation neglect the contribution of the sample confining wall on the pressure drop. The large dimensions of the samples adopted for the experimental

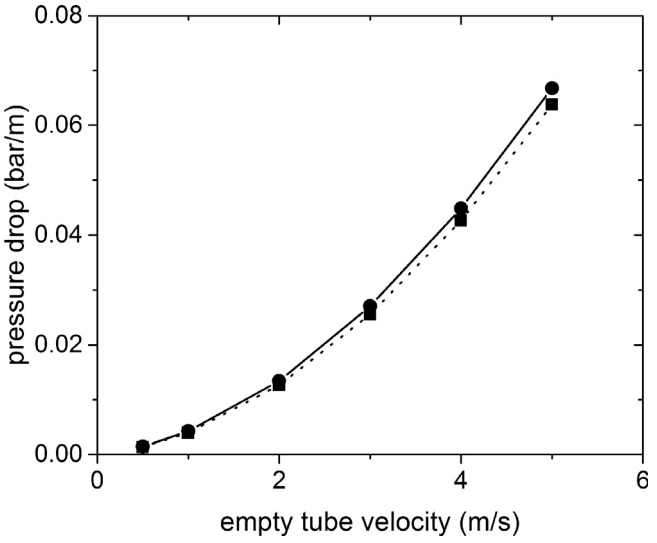

Fig. 10. Pressure drop as function of the empty tube velocity for Sample B by simulating digital (continuous line with circular symbols) and tomographic (dotted line with square symbols) reconstruction of foam structure.

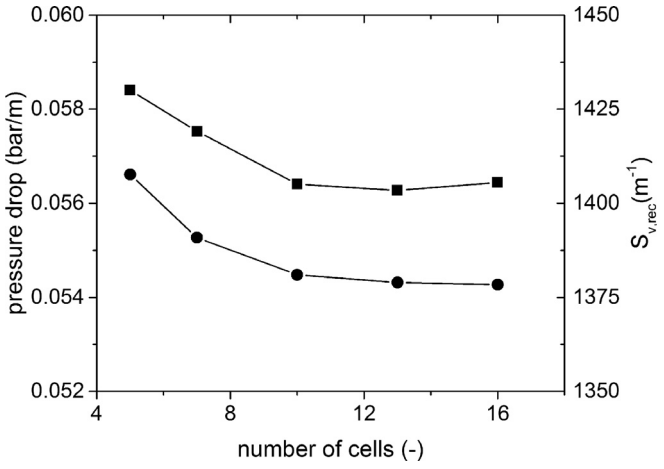

Fig. 9. Pressure drops (circle) and specific surface area (square) as a function of the number of cells in stream-wise direction for Sample E at an empty tube velocity of 2 m/s.

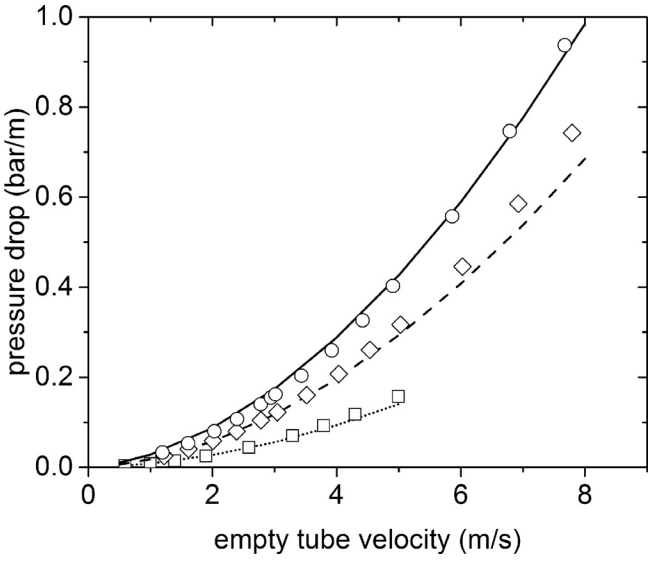

Fig. 11. Comparison of CFD simulations (lines) of pressure drop and experimental values (symbols) [50,61] for Samples E (dotted line – square symbol), H (dashed line – diamond symbol) and I (continuous line – circle symbol).

activity (several times the REV) would determine that this contribution, in particular for low-porosity foam, becomes negligible in respect to the loss due to the foam structure. The inertial contribution to the pressure drop (related to the form drag), which is prevalently related to the changes in the direction of the flow stream due to the presence of the solid matrix, is dominant at high flow velocities. In this view, one possible reason of such a deviation is the presence of closed pores due to the manufacturing process, whose effect is more evident at high flow rates. Furthermore, the real foam sample could exhibit a rough surface due to the manufacturing process, which could also affect the pressure loss [39]. The simulated foams have a perfectly smooth surface and no roughness has been taken into account.

In Fig. 12, the numerically evaluated pressure drops for the reconstructed samples are reported along with the experimental data and the predictions of some of the correlations available in the open literature [74–77]. The values obtained by simulating the reconstructed foams are usually in better agreement with data then the correlations. Thus, the reconstruction procedure is also an interesting tool in the design of such structures, since it might be used to investigate the performance of a collection of different foam samples, with reliable results in the context of the transport properties, without the necessity of really manufacturing many different foam samples.

4. Conclusions

We proposed a systematic methodology to virtually generate foam structures, which faithfully reproduce the geometrical properties of real foams samples, starting from a few pieces of geometrical information, i.e. the cell diameter and the void fraction. It is worth emphasizing that these parameters are easy to measure by optical microscopy and pycnometry techniques, respectively. The foam skeleton is generated by means of the Voronoi tessellation, which provides an interesting first guess for the foam structure. For the generation of the full geometry, we take into account the different cross-sectional shapes of the struts along with the clustering of the solid material at the nodes. The geometrical properties of reconstructed foams have been validated against experimental data obtained by μCT or MRI, obtaining good agreement for both the structural features and the specific surface areas. Moreover, pressure drop simulations clearly confirm the adequacy of the reconstructed foam for describing the complex flow field experienced in open-cell foams. Due to the analogies in the transport mechanisms, the adequacy of the reconstructed geometry for the CFD prediction of the pressure drop poses the basis for further investigation on the fluid-solid heat and mass transport properties. In this perspective, we plan to investigate heat and mass transport processes prevailing in these structures by means of the geometry

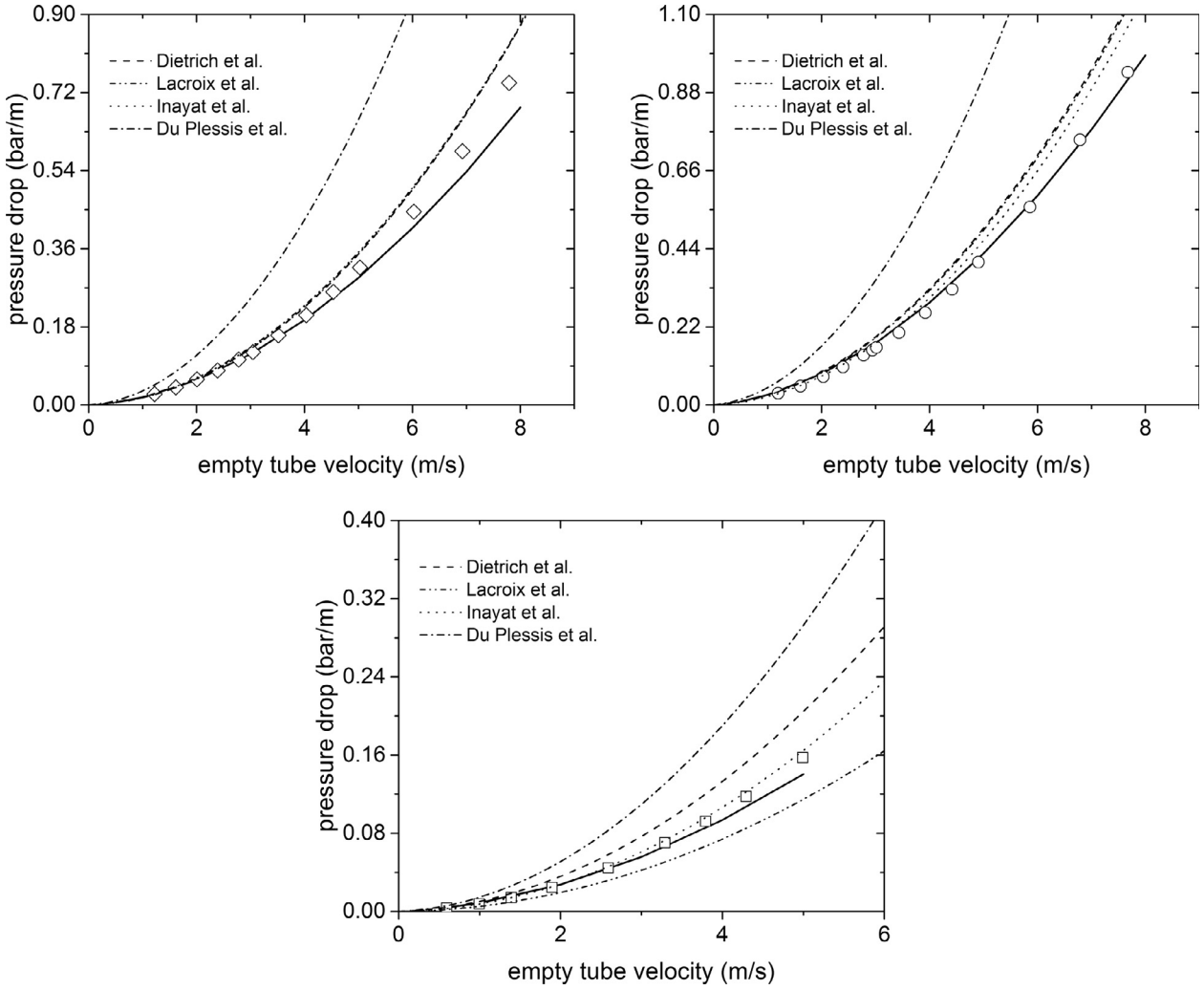

Fig. 12. Comparison between experiments (symbol), CFD simulations (continuous line) and pressure drops correlations (dashed lines) [71–74] for Samples E (square), H (diamond), I (circle).

generated by this methodology. Nevertheless, the methodology could be further improved in order to introduce the capability of generating concave struts, which can be found in metal foams characterized by extremely high porosities.

Our procedure allows, therefore, for the generation of virtual foam structures with similar properties to those of real open-cell foams. The procedure could be then exploited to perform advanced design of the foam structure, since it enables virtual testing of a large set of foams in order to figure out the optimal properties for the specific process requirements.

Acknowledgements

The research leading to these results has received funding from the European Research Council under the European Union's Horizon 2020 research and innovation programme (Grant Agreement no. 694910/INTENT). Computational time at CINECA (Bologna, Italy) is gratefully acknowledged.

References

[1] L. Giani, G. Groppi, E. Tronconi, Mass-transfer characterization of metallic foams as supports for structured catalysts, Ind. Eng. Chem. Res. 44 (2005) 4993–5002, http://dx.doi.org/10.1021/ie0490886.
[2] L. Giani, G. Groppi, E. Tronconi, Heat transfer characterisation of metallic foams, Ind. Eng. Chem. Res. 44 (2005) 9078–9085.
[3] E. Bianchi, T. Heidig, C.G. Visconti, G. Groppi, H. Freund, E. Tronconi, Heat transfer properties of metal foam supports for structured catalysts: wall heat transfer coefficient, Catal. Today 216 (2013) 121–134, http://dx.doi.org/10.1016/j.cattod.2013.06.019.
[4] A. Bhattacharya, V.V. Calmidi, R.L. Mahajan, Thermophysical properties of high porosity metal foams, Int. J. Heat Mass Transf. 45 (2002) 1017–1031, http://dx.doi.org/10.1016/S0017-9310(01)00220-4.
[5] B.R. Coquard, M. Loretz, D. Baillis, Conductive heat transfer in metallic/ceramic open-cell foams, Adv. Eng. Mater. (2008) 323–337, http://dx.doi.org/10.1002/adem.200700331.
[6] I. Ghosh, Heat transfer correlation for high-porosity open-cell foam, Int. J. Heat Mass Transf. 52 (2009) 1488–1494, http://dx.doi.org/10.1016/j.ijheatmasstransfer.2008.07.047.
[7] M.V. Twigg, J.T. Richardson, Fundamentals and applications of structured ceramic foam catalysts, Ind. Eng. Chem. Res. 46 (2007) 4166–4177, http://dx.doi.org/10.1021/ie061122o.
[8] A. Donazzi, M. Maestri, B.C. Michael, A. Beretta, P. Forzatti, G. Groppi, E. Tronconi, L.D. Schmidt, D.G. Vlachos, Microkinetic modeling of spatially resolved autothermal CH4 catalytic partial oxidation experiments over Rh-coated foams, J. Catal. 275 (2010) 270–279, http://dx.doi.org/10.1016/j.jcat.2010.08.007.
[9] R. Horn, N.J. Degenstein, K.A. Williams, L.D. Schmidt, Spatial and temporal profiles in millisecond partial oxidation processes, Catal. Lett. 110 (2006) 169–178, http://dx.doi.org/10.1007/s10562-006-0117-8.
[10] E. Verlato, S. Barison, S. Cimino, F. Dergal, L. Lisi, G. Mancino, M. Musiani, L. Vàzquez-Gòmez, Catalytic partial oxidation of methane over nanosized Rh supported on Fecralloy foams, Int. J. Hydrogen Energy 39 (2014) 11473–11485, http://dx.doi.org/10.1016/j.ijhydene.2014.05.076.
[11] P.S. Roy, N.K. Park, K. Kim, Metal foam-supported Pd-Rh catalyst for steam methane reforming and its application to SOFC fuel processing, Int. J. Hydrogen Energy 39 (2014) 4299–4310, http://dx.doi.org/10.1016/j.ijhydene.2014.01.004.
[12] A. Sirijaruphan, J.G. Goodwin, R.W. Rice, D. Wei, K.R. Butcher, G.W. Roberts, J.J. Spivey, Effect of metal foam supports on the selective oxidation of CO on Fe-promoted Pt/γ-Al2O3, Appl. Catal., A: Gen. 281 (2005) 11–18, http://dx.doi.org/10.1016/j.apcata.2004.11.006.
[13] A. Sirijaruphan, J.G. Goodwin, R.W. Rice, D. Wei, K.R. Butcher, G.W. Roberts, J.J. Spivey, Metal foam supported Pt catalysts for the selective oxidation of CO in hydrogen, Appl. Catal., A: Gen. 281 (2005) 1–9, http://dx.doi.org/10.1016/j.apcata.2004.10.019.
[14] Y. Liu, D. Edouard, L.D. Nguyen, D. Begin, P. Nguyen, C. Pham, C. Pham-Huu, High performance structured platelet milli-reactor filled with supported cobalt open cell SiC foam catalyst for the Fischer-Tropsch synthesis, Chem. Eng. J. 222 (2013) 265–273, http://dx.doi.org/10.1016/j.cej.2013.02.066.
[15] A. Montebelli, C.G. Visconti, G. Groppi, E. Tronconi, C. Ferreira, S. Kohler, Enabling small-scale methanol synthesis reactors through the adoption of highly conductive structured catalysts, Catal. Today 215 (2013) 176–185, http://dx.doi.org/10.1016/j.cattod.2013.02.020.
[16] A. Montebelli, C.G. Visconti, G. Groppi, E. Tronconi, S. Kohler, H.J. Venvik, R. Myrstad, Washcoating and chemical testing of a commercial Cu/ZnO/Al_2O_3 catalyst for the methanol synthesis over copper open-cell foams, Appl. Catal., A: Gen. 481 (2014) 96–103, http://dx.doi.org/10.1016/j.apcata.2014.05.005.
[17] I. Gräf, G. Ladenburger, B. Kraushaar-Czarnetzki, Heat transport in catalytic sponge packings in the presence of an exothermal reaction: characterization by 2D modeling of experiments, Chem. Eng. J. 287 (2016) 425–435, http://dx.doi.org/10.1016/j.cej.2015.11.042.
[18] D. Edouard, M. Lacroix, C.P. Huu, F. Luck, Pressure drop modeling on SOLID foam: state-of-the art correlation, Chem. Eng. J. 144 (2008) 299–311, http://dx.doi.org/10.1016/j.cej.2008.06.007.
[19] X. Fan, X. Ou, F. Xing, G.A. Turley, P. Denissenko, M.A. Williams, N. Batail, C. Pham, A.A. Lapkin, Microtomography-based numerical simulations of heat transfer and fluid flow through β-SiC open-cell foams for catalysis, Catal. Today (2015), http://dx.doi.org/10.1016/j.cattod.2015.12.012.
[20] A. Diani, K.K. Bodla, L. Rossetto, S.V. Garimella, Numerical investigation of pressure drop and heat transfer through reconstructed metal foams and comparison against experiments, Int. J. Heat Mass Transf. 88 (2015) 508–515, http://dx.doi.org/10.1016/j.ijheatmasstransfer.2015.04.038.
[21] P. Ranut, E. Nobile, L. Mancini, High resolution microtomography-based CFD simulation of flow and heat transfer in aluminum metal foams, Appl. Therm. Eng. 69 (2014) 230–240, http://dx.doi.org/10.1016/j.applthermaleng.2013.11.056.
[22] P. Kumar, F. Topin, J. Vicente, Determination of effective thermal conductivity from geometrical properties: application to open cell foams, Int. J. Therm. Sci. 81 (2014) 13–28, http://dx.doi.org/10.1016/j.ijthermalsci.2014.02.005.
[23] W. Thomson, On the division of space with minimum partional area, Philos. Mag. 24 (1887) 503.
[24] D. Weaire, The Kelvin Problem: Foam Structures of Minimal Surface Area, CRC Press, 1997.
[25] J. Von Rickenbach, F. Lucci, C. Narayanan, P. Dimopoulos Eggenschwiler, D. Poulikakos, Multi-scale modelling of mass transfer limited heterogeneous reactions in open cell foams, Int. J. Heat Mass Transf. 75 (2014) 337–346, http://dx.doi.org/10.1016/j.ijheatmasstransfer.2014.03.060.
[26] A. Della Torre, F. Lucci, G. Montenegro, A. Onorati, P. Dimopoulos Eggenschwiler, E. Tronconi, G. Groppi, CFD modeling of catalytic reactions in open-cell foam substrates, Comput. Chem. Eng. 92 (2016) 55–63, http://dx.doi.org/10.1016/j.compchemeng.2016.04.031.
[27] T. Horneber, C. Rauh, A. Delgado, Numerical simulations of fluid dynamics in carrier structures for catalysis: characterization and need for optimization, Chem. Eng. Sci. 117 (2014) 229–238, http://dx.doi.org/10.1016/j.ces.2014.06.036.
[28] A. Inayat, H. Freund, T. Zeiser, W. Schwieger, Determining the specific surface area of ceramic foams: the tetrakaidecahedra model revisited, Chem. Eng. Sci. 66 (2011) 1179–1188, http://dx.doi.org/10.1016/j.ces.2010.12.031.
[29] N.J. Mills, The wet Kelvin model for air flow through open-cell polyurethane foams, J. Mater. Sci. 40 (2005) 5845–5851, http://dx.doi.org/10.1007/s10853-005-5018-5.
[30] D. Weaire, R. Phelan, A counter-example to Kelvin's conjecture on minimal surfaces, Philos. Mag. Lett. 69 (1994) 107–110, http://dx.doi.org/10.1080/09500839408241577.
[31] K. Boomsma, D. Poulikakos, Y. Ventikos, Simulations of flow through open cell metal foams using an idealized periodic cell structure, Int. J. Heat Fluid Flow 24 (2003) 825–834, http://dx.doi.org/10.1016/j.ijheatfluidflow.2003.08.002.
[32] T. Truong Huu, M. Lacroix, C. Pham Huu, D. Schweich, D. Edouard, Towards a more realistic modeling of solid foam: use of the pentagonal dodecahedron geometry, Chem. Eng. Sci. 64 (2009) 5131–5142, http://dx.doi.org/10.1016/j.ces.2009.08.028.
[33] P. Habisreuther, N. Djordjevic, N. Zarzalis, Statistical distribution of residence time and tortuosity of flow through open-cell foams, Chem. Eng. Sci. 64 (2009) 4943–4954, http://dx.doi.org/10.1016/j.ces.2009.07.033.
[34] F. Lucci, A. Della Torre, J. von Rickenbach, G. Montenegro, D. Poulikakos, P. Dimopoulos Eggenschwiler, Performance of randomized Kelvin cell structures as catalytic substrates: mass-transfer based analysis, Chem. Eng. Sci. 112 (2014) 143–151, http://dx.doi.org/10.1016/j.ces.2014.03.023.
[35] L.J. Gibson, M.F. Ashby, Cellular Solids: Structure and Properties, Cambridge University Press, 1999.
[36] A.M. Kraynik, D. Reinelt, F. van Swol, Structure of random monodisperse foam, Phys. Rev. E. Stat. Nonlin. Soft Matter Phys. 67 (2003), http://dx.doi.org/10.1103/PhysRevE.67.031403 031403.
[37] A.P. Roberts, E.J. Garboczi, Elastic properties of model random three-dimensional open-cell solid, J. Mech. Phys. Solids 50 (2002) 33–55, http://dx.doi.org/10.1016/S0022-5096(01)00056-4.
[38] J. Randrianalisoa, D. Baillis, C.L. Martin, R. Dendievel, Microstructure effects on thermal conductivity of open-cell foams generated from the Laguerre-Voronoï tessellation method, Int. J. Therm. Sci. 98 (2015) 277–286, http://dx.doi.org/10.1016/j.ijthermalsci.2015.07.016.
[39] C. Hutter, A. Zenklusen, S. Kuhn, P. Rudolf von Rohr, Large eddy simulation of flow through a streamwise-periodic structure, Chem. Eng. Sci. 66 (2011) 519–529, http://dx.doi.org/10.1016/j.ces.2010.11.015.
[40] S. Kanaun, O. Tkachenko, Effective conductive properties of open-cell foams, Int. J. Eng. Sci. 46 (2008) 551–571, http://dx.doi.org/10.1016/j.ijengsci.2008.01.012.
[41] E. Bianchi, T. Heidig, C.G. Visconti, G. Groppi, H. Freund, E. Tronconi, An appraisal of the heat transfer properties of metallic open-cell foams for strongly exo-/endo-thermic catalytic processes in tubular reactors, Chem. Eng. J. 198–199 (2012) 512–528, http://dx.doi.org/10.1016/j.cej.2012.05.045.
[42] G.D. Wehinger, T. Eppinger, M. Kraume, Detailed numerical simulations of catalytic fixed-bed reactors: heterogeneous dry reforming of methane, Chem. Eng. Sci. 122 (2015) 197–209, http://dx.doi.org/10.1016/j.ces.2014.09.007.
[43] M.J. Baker, G.R. Tabor, Computational analysis of transitional air flow through packed columns of spheres using the finite volume technique, Comput. Chem.

Eng. 34 (2010) 878–885, http://dx.doi.org/10.1016/j.compchemeng.2009.10.013.
[44] H. Freund, T. Zeiser, F. Huber, E. Klemm, G. Brenner, F. Durst, G. Emig, Numerical simulations of single phase reacting flows in randomly packed fixed-bed reactors and experimental validation, Chem. Eng. Sci. 58 (2003) 903–910, http://dx.doi.org/10.1016/S0009-2509(02)00622-X.
[45] C. Kloss, C. Goniva, A. Hager, S. Amberger, S. Pirker, Models, algorithms and validation for opensource DEM and CFD-DEM, Prog. Comput. Fluid Dyn. 12 (2012) 140–152, http://dx.doi.org/10.1504/PCFD.2012.047457.
[46] S. Ookawara, M. Kuroki, D. Street, K. Ogawa, High-fidelity DEM-CFD modeling of packed bed reactors for process intensification, Proc. Eur. Congr. Chem. Eng. (2007) 16–20.
[47] A. De Klerk, Voidage variation in packed beds at small column to particle diameter ratio, AIChE J. 49 (2003) 2022–2029, http://dx.doi.org/10.1002/aic.690490812.
[48] R.P. Zou, A.B. Yu, The packing of spheres in a cylindrical container: the thickness effect, Chem. Eng. Sci. 50 (1995) 1504–1507, http://dx.doi.org/10.1016/0009-2509(94)00483-8.
[49] C.H. Rycroft, VORO++: a three-dimensional Voronoi cell library in C++, Chaos 19 (2009) 24–25, http://dx.doi.org/10.1063/1.3215722.
[50] E. Brun, J. Vicente, F. Topin, R. Occelli, M.J. Clifton, Microstructure and transport properties of cellular materials: representative volume element, Adv. Eng. Mater. 11 (2009) 805–810, http://dx.doi.org/10.1002/adem.200900131.
[51] J.A.F. Plateau, Experimental and Theoretical Static of Liquids Subject to Molecular Forces Only, 1873.
[52] G. Incera Garrido, F.C. Patcas, S. Lang, B. Kraushaar-Czarnetzki, Mass transfer and pressure drop in ceramic foams: a description for different pore sizes and porosities, Chem. Eng. Sci. 63 (2008) 5202–5217, http://dx.doi.org/10.1016/j.ces.2008.06.015.
[53] J. Grosse, B. Dietrich, G. Incera Garrido, P. Habisreuther, N. Zarzalis, H. Martin, M. Kind, B. Kraushaar-Czarnetzki, Morphological characterization of ceramic sponges for applications in chemical engineering, Ind. Eng. Chem. Res. 48 (2009) 10395–10401, http://dx.doi.org/10.1021/ie900651c.
[54] B. Dietrich, W. Schabel, M. Kind, H. Martin, Pressure drop measurements of ceramic sponges-determining the hydraulic diameter, Chem. Eng. Sci. 64 (2009) 3633–3640, http://dx.doi.org/10.1016/j.ces.2009.05.005.
[55] C. T'Joen, P. De Jaeger, H. Huisseune, S. Van Herzeele, N. Vorst, M. De Paepe, Thermo-hydraulic study of a single row heat exchanger consisting of metal foam covered round tubes, Int. J. Heat Mass Transf. 53 (2010) 3262–3274, http://dx.doi.org/10.1016/j.ijheatmasstransfer.2010.02.055.
[56] E.N. Schmierer, A. Razani, Self-consistent open-celled metal foam model for thermal applications, J. Heat Transfer. 128 (2006) 1194, http://dx.doi.org/10.1115/1.2352787.
[57] S. Kumar, S.K. Kurtz, Simulation of material microstructure using a 3D voronoi tesselation: calculation of effective thermal expansion coefficient of polycrystalline materials, Acta Metall. Mater. 42 (1994) 3917–3927, http://dx.doi.org/10.1016/0956-7151(94)90170-8.
[58] M.D. Montminy, A.R. Tannenbaum, C.W. Macosko, The 3D structure of real polymer foams, J. Colloid Interface Sci. 280 (2004) 202–211, http://dx.doi.org/10.1016/j.jcis.2004.07.032.
[59] C. Perrot, R. Panneton, X. Olny, Periodic unit cell reconstruction of porous media: application to open-cell aluminum foams, J. Appl. Phys. 101 (2007), http://dx.doi.org/10.1063/1.2745095.
[60] L. Gong, S. Kyriakides, W.Y. Jang, Compressive response of open-cell foams. Part I: morphology and elastic properties, Int. J. Solids Struct. 42 (2005) 1355–1379, http://dx.doi.org/10.1016/j.ijsolstr.2004.07.023.
[61] T. Dillard, F. N'guyen, E. Maire, L. Salvo, S. Forest, Y. Bienvenu, J.-D. Bartout, M. Croset, R. Dendievel, P. Cloetens, 3D quantitative image analysis of open-cell nickel foams under tension and compression loading using X-ray microtomography, Philos. Mag. 85 (2005) 2147–2175, http://dx.doi.org/10.1080/14786430412331331916.
[62] S. De Schampheleire, P. De Jaeger, K. De Kerpel, B. Ameel, H. Huisseune, M. De Paepe, How to study thermal applications of open-cell metal foam: experiments and computational fluid dynamics, Materials (Basel) 9 (2016) 1–27, http://dx.doi.org/10.3390/ma9020094.
[63] R. Al-Raoush, Microstructure characterization of granular materials, Phys. A: Stat. Mech. Appl. 377 (2007) 545–558, http://dx.doi.org/10.1016/j.physa.2006.11.090.
[64] A. Inayat, H. Freund, A. Schwab, T. Zeiser, W. Schwieger, Predicting the specific surface area and pressure drop of reticulated ceramic foams used as catalyst support, Adv. Eng. Mater. 13 (2011) 990–995, http://dx.doi.org/10.1002/adem.201100038.
[65] P. De Jaeger, C. T'Joen, H. Huisseune, B. Ameel, M. De Paepe, An experimentally validated and parameterized periodic unit-cell reconstruction of open-cell foams, J. Appl. Phys. 109 (2011), http://dx.doi.org/10.1063/1.3587159.
[66] M.H.J. Pedras, M.J.S. de Lemos, Macroscopic turbulence modeling for incompressible flow through undeformable porous media, Int. J. Heat Mass Transf. 44 (2001) 1081–1093, http://dx.doi.org/10.1016/S0017-9310(00)00202-7.
[67] Y. Jin, M.-F. Uth, A.V. Kuznetsov, H. Herwig, Numerical investigation of the possibility of macroscopic turbulence in porous media: a direct numerical simulation study, J. Fluid Mech. 766 (2015) 76–103, http://dx.doi.org/10.1017/jfm.2015.9.
[68] S. Meinicke, C.O. Möller, B. Dietrich, M. Schlüter, T. Wetzel, Experimental and numerical investigation of single-phase hydrodynamics in glass sponges by means of combined μPIV measurements and CFD simulation, Chem. Eng. Sci. 160 (2017) 131–143, http://dx.doi.org/10.1016/j.ces.2016.11.027.
[69] A. Della Torre, G. Montenegro, G.R. Tabor, M.L. Wears, CFD characterization of flow regimes inside open cell foam substrates, Int. J. Heat Fluid Flow. 50 (2014) 72–82, http://dx.doi.org/10.1016/j.ijheatfluidflow.2014.05.005.
[70] H.G. Weller, G. Tabor, H. Jasak, C. Fureby, A tensorial approach to computational continuum mechanics using object-oriented techniques, Comput. Phys. 12 (1998) 620–631, http://dx.doi.org/10.1063/1.168744.
[71] S. Patankar, Numerical heat transfer and fluid flow, Ser. Comput. Methods Mech. Therm. Sci. (1980).
[72] F. Menter, T. Esch, Elements of industrial heat transfer predictions, in: 16th Brazilian Congr. Mech. Eng., 2001: pp. 26–30.
[73] F.R. Menter, M. Kuntz, R. Langtry, Ten years of industrial experience with the SST turbulence model, Turbul. Heat Mass Transf. 4 (4) (2003) 625–632.
[74] A. Inayat, M. Klumpp, M. Lämmermann, H. Freund, W. Schwieger, Development of a new pressure drop correlation for open-cell foams based completely on theoretical grounds: taking into account strut shape and geometric tortuosity, Chem. Eng. J. 287 (2016) 704–719, http://dx.doi.org/10.1016/j.cej.2015.11.050.
[75] B. Dietrich, Pressure drop correlation for ceramic and metal sponges, Chem. Eng. Sci. 74 (2012) 192–199, http://dx.doi.org/10.1016/j.ces.2012.02.047.
[76] M. Lacroix, P. Nguyen, D. Schweich, C. Pham Huu, S. Savin-Poncet, D. Edouard, Pressure drop measurements and modeling on SiC foams, Chem. Eng. Sci. 62 (2007) 3259–3267, http://dx.doi.org/10.1016/j.ces.2007.03.027.
[77] P. Du Plessis, A. Montillet, J. Comiti, J. Legrand, Pressure drop prediction for flow through high porosity metallic foams, Chem. Eng. Sci. 49 (1994) 3545–3553.